



# Spatiotemporal analysis identifies ABF2 and ABF3 as key hubs of endodermal response to nitrate

Orlando Contreras-López<sup>a,b,1</sup>, Elena A. Vidal<sup>c,d,e,1</sup>, Eleodoro Riveras<sup>a,b,c,1</sup>, José M. Alvarez<sup>c,d,1</sup>, Tomás C. Moyano<sup>a,b,c,1</sup>, Erin E. Sparks<sup>f</sup>, Joaquín Medina<sup>g</sup>, Angelo Pasquino<sup>h</sup>, Philip N. Benfey<sup>i,j</sup>, Gloria M. Coruzzi<sup>h</sup>, and Rodrigo A. Gutiérrez<sup>a,b,c,2</sup>

<sup>a</sup>Fondo de Desarrollo de Areas Prioritarias, Center for Genome Regulation, 8370415 Santiago, Chile; <sup>b</sup>Departamento de Genética Molecular y Microbiología, Facultad de Ciencias Biológicas, Pontificia Universidad Católica de Chile, 8331010 Santiago, Chile; <sup>c</sup>Agencia Nacional de Investigación y Desarrollo–Millennium Science Initiative Program, Millennium Institute for Integrative Biology, 7500565 Santiago, Chile; <sup>d</sup>Centro de Genómica y Bioinformática, Facultad de Ciencias, Universidad Mayor, 8580745 Santiago, Chile; <sup>e</sup>Escuela de Biotecnología, Facultad de Ciencias, Universidad Mayor, 8580745 Santiago, Chile; <sup>f</sup>Department of Plant and Soil Sciences, Delaware Biotechnology Institute, University of Delaware, Newark, DE 19713; <sup>g</sup>Centro de Biotecnología y Genómica de Plantas, Instituto Nacional de Investigación y Tecnología Agraria y Alimentaria, Universidad Politécnica de Madrid, 28040 Madrid, Spain; <sup>h</sup>Center for Genomics and Systems Biology, New York University, New York, NY 10003; <sup>i</sup>Department of Biology, Duke University, Durham, NC 27708; and <sup>j</sup>HHMI, Duke University, Durham, NC 27708

Edited by Julia Bailey-Serres, Department of Botany and Plant Sciences, University of California, Riverside, CA; received April 26, 2021; accepted December 14, 2021

**Nitrate is a nutrient and a potent signal that impacts global gene expression in plants. However, the regulatory factors controlling temporal and cell type-specific nitrate responses remain largely unknown. We assayed nitrate-responsive transcriptome changes in five major root cell types of the *Arabidopsis thaliana* root as a function of time. We found that gene-expression response to nitrate is dynamic and highly localized and predicted cell type-specific transcription factor (TF)-target interactions. Among cell types, the endodermis stands out as having the largest and most connected nitrate-regulatory gene network. ABF2 and ABF3 are major hubs for transcriptional responses in the endodermis cell layer. We experimentally validated TF-target interactions for ABF2 and ABF3 by chromatin immunoprecipitation followed by sequencing and a cell-based system to detect TF regulation genome-wide. Validated targets of ABF2 and ABF3 account for more than 50% of the nitrate-responsive transcriptome in the endodermis. Moreover, ABF2 and ABF3 are involved in nitrate-induced lateral root growth. Our approach offers an unprecedented spatiotemporal resolution of the root response to nitrate and identifies important components of cell-specific gene regulatory networks.**

cell-specific | nitrate signaling | transcriptional regulation

Nitrogen (N) is an essential macronutrient and a potent signal for plant growth and development. Nitrate is a main source of this nutrient in most soils (1); however, its availability is often limiting, negatively affecting plant growth and development, as well as crop yield. To cope with this nutritional limitation, plants can modify their root system architecture (RSA) to optimize nitrate acquisition from soils. In this context, nitrate availability controls growth and development of primary roots (PRs), lateral roots (LRs), and root hairs (2–5).

The transcriptome response of roots to nitrate includes a rapid regulation of thousands of genes involved in biological processes related to nitrate transport and metabolism, hormone signaling, and organ growth and development (6–11). Considerable efforts have been devoted in the last years to identify transcription factors (TFs) and regulatory networks that control nitrate responses. A regulatory network for N-associated metabolism was constructed using enhanced yeast one-hybrid (Y1H) assays (10). Screening for TF binding to promoters of genes involved in N-related process, C-metabolism and transport, organ growth, and hormonal responses identified 21 TFs controlling different aspects of N metabolism, with relevant roles in root and shoot growth (10). The generation of detailed time-series transcriptomics studies, combined with machine-learning approaches, have established gene regulatory network (GRN) models of the dynamic shoot and root responses to changes in N availability

(6, 7, 11). Combination of these temporal transcriptomics data with regulatory TF-target interactions obtained from the TF perturbation assay Transient Assay Reporting Genome-wide Effects of Transcription factors (TARGET) validated inferred regulatory interactions and provided network charts linking early and late regulatory events of the root nitrate response. In addition, integration of global gene expression, RNA polymerase II occupancy, and chromatin accessibility information has provided insights into the transcriptional wiring and hierarchical contribution of previously identified TFs, as well as new TFs controlling the root response to nitrate (11). Moreover, genome-wide gene expression and TF-target interactions obtained from TARGET and chromatin immunoprecipitation sequencing (ChIP-seq) have validated direct and indirect targets of TGA1, a previously described TF involved in the root nitrate response (12, 13), and established that TGA1 acts as a controller of the transcriptional

## Significance

**We analyzed the nitrate-responsive transcriptome of the *Arabidopsis thaliana* root at a spatial and temporal resolution. Our work provides evidence that the response to nitrate is dynamic and highly localized, orchestrating a root response that is finely coordinated in space and time. Gene regulatory network analysis allowed for identification of the endodermis as a cell type enriched in regulatory interactions, with ABF2 and ABF3 transcription factors acting as key regulators of gene expression in the endodermis and lateral root growth in response to nitrate. Our results provide a comprehensive catalog of root nitrate-responsive genes at an unprecedented resolution and contribute to understanding how organisms sense and respond to environmental cues, coordinating cell-specific responses into organ development.**

Author contributions: O.C.-L., E.A.V., and R.A.G. designed research; O.C.-L., E.A.V., E.R., J.M.A., T.C.M., E.E.S., and A.P. performed research; J.M., P.N.B., and G.M.C. contributed new reagents/analytic tools; O.C.-L., E.A.V., E.R., J.M.A., T.C.M., E.E.S., and A.P. analyzed data; J.M., P.N.B., and G.M.C. contributed to data interpretation and manuscript drafting; and O.C.-L., E.A.V., E.R., J.M.A., T.C.M., and R.A.G. wrote the paper.

The authors declare no competing interest.

This article is a PNAS Direct Submission.

This article is distributed under Creative Commons Attribution-NonCommercial-NoDerivatives License 4.0 (CC BY-NC-ND).

<sup>1</sup>O.C.-L., E.A.V., E.R., J.M.A., and T.C.M. contributed equally to this work.

<sup>2</sup>To whom correspondence may be addressed. Email: rgutierrez@bio.puc.cl.

This article contains supporting information online at <http://www.pnas.org/lookup/suppl/doi:10.1073/pnas.2107879119/-DCSupplemental>.

Published January 19, 2022.

rate response to different nitrate concentrations, coordinating nutrient availability and root growth (8). More recently, a combination of transcriptomics, TARGET, and DamID-seq data identified a hit-and-run mechanism of transcriptional control in response to nitrate driven by NLP7 (14), one of the main components of the nitrate signaling pathway (15–18), impacting plant biomass and PR growth (14).

One common limitation of such genome-wide studies is that most represent TF–DNA interactions occurring at a whole-organ level. However, the handful of studies that have assayed cell type-specific expression patterns in roots have shown that different cell types have unique transcriptional profiles, and that different cell types respond to nitrate in unique ways (19, 20). Using *Arabidopsis* lines expressing green fluorescent protein (GFP) in specific cell types of the root and FACS, a transcriptome map was generated from external and internal root layers, including the LR cap, epidermis–cortex, endodermis–pericycle, pericycle, and stele cells after a 2-h nitrate provision to ammonium-grown seedlings (19). This work showed that the number of regulated genes and the biological processes evoked by nitrate greatly depend on the cell type analyzed, showing that the nitrate response is spatially discrete (19). However, only a single time point was analyzed, which limits the discovery of gene relationships and consequently the construction of cell-specific GRNs. In order to capture the temporal and spatial components of the N response, a 48-h time series of ammonium nitrate treatments was performed in cortex and pericycle cells (20). In this study, the authors found that although N-responsive genes are cell- and time-specific, N-responsive biological processes are regulated by a common core of N-regulated TFs in the cortex and pericycle (20). This study focused on two cell types, and the time points captured in the analysis (hours) focused on long-term changes and did not capture early signaling events and rapid responses to nitrate (minutes) (20).

To gain insights into the early signaling events occurring at the cellular level in response to nitrate in roots, we analyzed the changes in the transcriptome after a short time-course of nitrate treatment (12 to 120 min) in five major cell types of the root: epidermis, cortex, endodermis, pericycle, and stele. We found that nitrate-responsive genes and known biological processes are coordinately regulated in time, initiating in the outermost cell layers and then propagating into innermost cell layers of the root. Integration of our transcriptomics data and published TF–DNA interaction data into a GRN model highlighted the endodermis as a regulatory hub of nitrate responses and identified the abscisic acid (ABA)–related transcription factors ABA RESPONSE ELEMENT BINDING/ABSCISIC ACID RESPONSIVE ELEMENT BINDING FACTOR (ABF)2 and ABF3 as key regulators of the endodermis responses to nitrate. Combining analysis of TF–target interactions from Y1H, ChIP-seq, and TARGET TF-perturbation assays in root cells, we found that ABF2 and ABF3 control a relevant proportion of nitrate-responsive genes in the endodermis. Moreover, we found that *abf2* and *abf3* mutant plants show an altered root response to nitrate, with a decreased density of LR. Our results indicate that ABF2 and ABF3 are key early cell type-specific regulatory factors of the nitrate response involved in the modulation of RSA.

## Results

**Spatiotemporal Analysis of the Root Nitrate Response.** To understand how the nitrate response is orchestrated across root cell types, as a function of time, we performed a spatiotemporal transcriptome analysis in the epidermis, cortex, endodermis, pericycle, and stele at 12, 20, 60, and 120 min after nitrate treatment (21). GFP-based reporter lines were used to isolate specific cell types using FACS (*Methods*). To validate our transcriptome data for individual cell types, we used the Pavlidis

Template Matching algorithm (22) to generate a list of genes whose expression is enriched in specific cell types, as previously described (23). This analysis shows that transcriptomes of specific cell types have been successfully isolated (*SI Appendix, Fig. S1* and *Dataset S1*). To determine if the protoplast isolation procedure had an effect on gene-expression levels, we compared global gene expression in the isolated cell types and in whole roots. We found a high correlation of gene-expression levels between cells and whole roots (Spearman correlation = 0.92) (*SI Appendix, Fig. S2*), indicating that the transcriptomic profile of the whole organ can be captured at the cellular level, as has been previously reported using single-cell analysis (24) and FACS (25, 26).

To identify genes that are differentially expressed after nitrate treatment in each cell type and time point, we performed a one-way ANOVA with a false-discovery rate (FDR) of 0.05. Genes that showed differential expression were subjected to a post hoc analysis. We obtained 5,231 genes that show differential expression in response to nitrate treatment in at least one of the five cell types in at least one time point analyzed (*Fig. 1A* and *Dataset S2*). Our approach allowed us to capture most of the nitrate-responsive genes reported in previous whole-root analyses (6–8, 11, 27, 28), as well as an important number of novel nitrate-responsive genes (*SI Appendix, Fig. S3*). This result highlights the increased resolution of the spatiotemporal analysis and the potential to uncover previously unidentified cell-specific transcriptional regulators of the nitrate response. A simple browser to visualize and download the data for specific genes is available at <http://virtualplant.bio.puc.cl/cgi-bin/Lab/celltype.cgi>.

During protoplast generation, root tissue was incubated with cell wall-degrading enzymes for a period of approximately 1 h. To assess a possible effect of this incubation time in the temporality of the nitrate response, we compared our data with a previous nitrate time-course experiment performed in whole roots (11) with the expression data obtained in this study. We found that the combined nitrate response of protoplasts over time closely resembles the nitrate response of whole roots (*SI Appendix, Fig. S4A*). Additionally, we analyzed the expression of four prototypical nitrate-responsive genes (*NRT1.1*, *NRT2.1*, *NIR*, and *TGA1*) in root protoplasts and whole roots exposed to 2 h of nitrate treatment or to 2 h plus 1 additional hour of nitrate treatment, to emulate the timing of the protoplast generation procedure. As shown in *SI Appendix, Fig. S4B*, the expression of these marker genes in root protoplasts is similar to the 2-h-treated whole roots, but differs from the expression in plants treated with nitrate for 3 h. These results indicate that the temporality of the nitrate response is not affected by the protoplast generation, and that our experimental design allowed us to capture early nitrate responses in root cells.

Nitrate elicited a rapid transcriptome reprogramming in all cell types assayed, with 1,572 genes responding 12 min after nitrate exposure (*Fig. 1A* and *Dataset S2*). A substantial fraction of the total number of nitrate-responsive genes are in the endodermal cell layer (2,205 genes, 42.5% of regulated genes), suggesting an important role for this tissue in the temporal nitrate response in roots (*Dataset S2*). A large fraction of genes was nitrate regulated in a single cell type (77.6% of the genes) (*Fig. 1B*) or at a single time point (76.6% of the genes) (*Fig. 1C*). These results are consistent with previous time- and cell type-specific analyses of the nitrate response (7, 19, 20), indicating that the nitrate response is organized by transient, highly localized cell type-specific regulation of transcripts.

To determine the impact of nitrate treatment on biological processes in the root, we performed gene ontology (GO) term enrichment analysis in each cell type at each time point using GStats (29) (*Dataset S3*). As shown in *Fig. 1D*, we found an ordered spatiotemporal regulation of biological processes over time. At 12 min, only the epidermis shows enriched biological

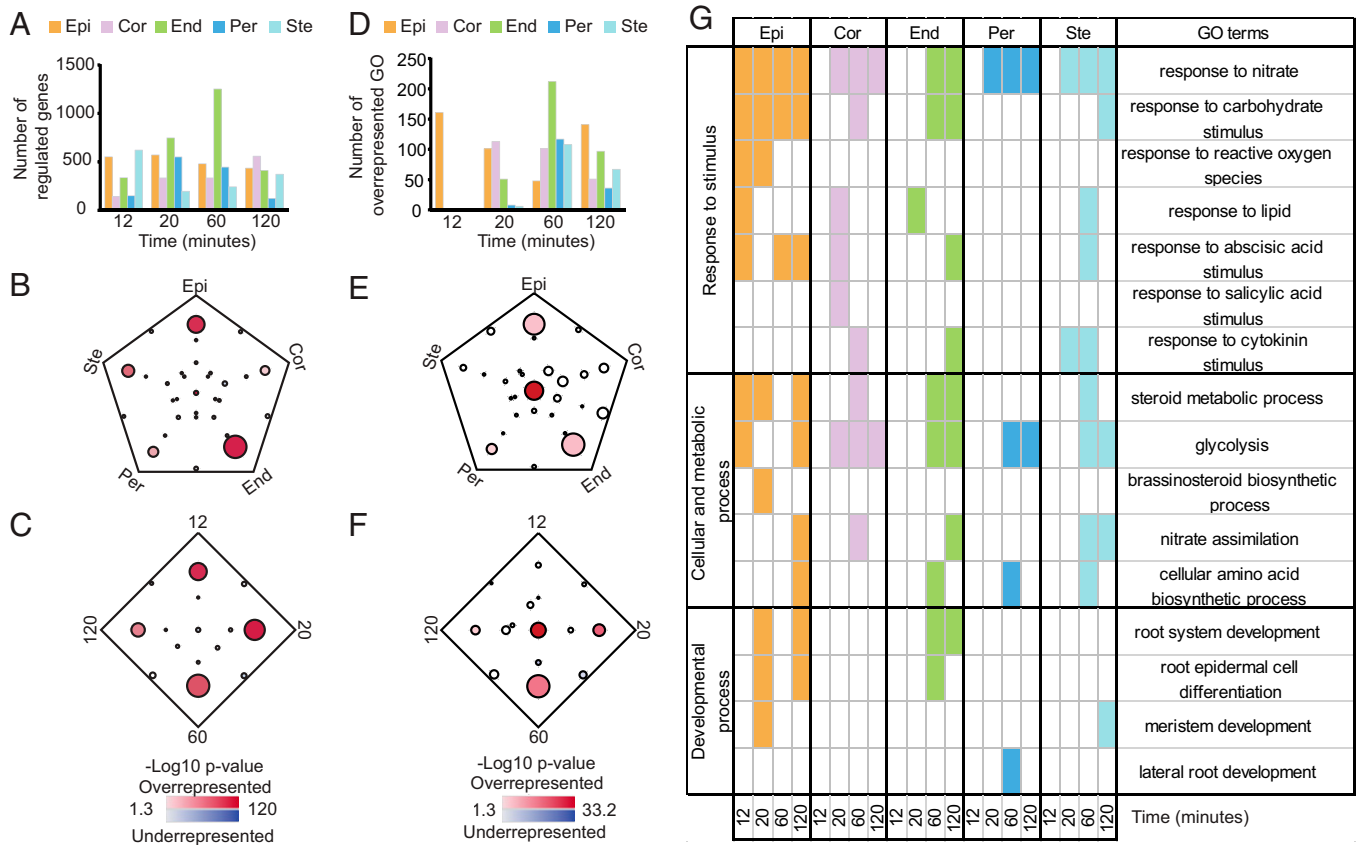


**Fig. 1.** Spatiotemporal analysis of gene expression in cells of the *Arabidopsis* root in response to nitrate. (A) Differentially expressed genes in response to nitrate treatment were determined from microarray data using a one-way ANOVA with an FDR cutoff of 0.05 followed by a post hoc analysis. We show the number of regulated genes in each time point and cell type. (B and C) The intersections between lists of regulated genes in each cell type (B) and time point (C) were determined using the SunGear tool (84). Each vertex of the polygons represents a cell type or time point and the intersections between gene sets are represented as circles. The significance of under- or overrepresentation (shown as the indicated color scale) in the number of genes in the intersections is estimated using a binomial test, which indicates whether a circle contains higher or lower overlap of genes than expected given the total number of genes by each of the queried analyses. (D) Overrepresented GO Biological Processes were determined for each list of differentially expressed genes using GOSTats (29) (FDR < 0.01, GO level 5). We show the number of overrepresented GO terms (level 5) for each cell type at each time point analyzed. (E and F) The intersections between lists of regulated genes in each cell type (E) and time point (F) were determined using the SunGear tool. (G) The presence (colored boxes) or absence (white boxes) of overrepresented GO terms (FDR < 0.01, GO level 5) in lists of differentially expressed genes in the five cell types at each time point. GO terms are arranged by parent GO terms (level 2). Cor: cortex; End: endodermis; Epi: epidermis; Per: pericycle; Ste: stele.

processes, indicating this tissue is the first to organize a coherent response of known function, consistent with its outermost position on the root. At 20 min, enriched GO terms are found mostly associated with external cells of the root (epidermis and cortex), while at later time points (60 and 120 min) we detected enrichment of GO terms in all five root cell types (Fig. 1D and Dataset S3). In contrast to the predominant cell- and time-specific regulation of genes, nitrate regulation of biological processes is more consistent across cell types and time points, as has been reported in previous analyses at the whole-root level (27) (Fig. 1E and F). Enriched biological processes shared by all cell types, and in most time points include “response to nitrate,” “anion transport,” “glycolysis,” “oxoacid metabolic process,” and “prosthetic group metabolic process,” indicating that these processes are rapidly and steadily activated across the root (Fig. 1G and Dataset S3). In contrast, processes related to root development, hormone responses, transport, and metabolism are nitrate-responsive only in a few cell types, and at a few time points, suggesting a localized and transient regulation in response to nitrate. For example, genes involved in LR development are overrepresented specifically in the pericycle after 60 min of nitrate treatment (Fig. 1G). This result is

consistent with the reported effect of nitrate in the control of LR growth (2, 4, 5, 19, 30).

**The Endodermis Has the Largest and Most Highly Connected Nitrate GRN.** To determine nitrate-responsive regulatory factors and GRNs at the level of cell type, we integrated the spatiotemporal transcriptomic data with regulatory information on TF–target gene interactions obtained from the Plant Cistrome Database (31), CIS-BP Database (Catalog of Inferred Sequence-Binding Peptides) (32), and the *Arabidopsis* Gene Regulatory Interaction Server (AGRIS) (33). Because of the transient and localized cell-type regulation of transcripts in response to nitrate (Fig. 1B and C), and to preserve the spatiotemporal nature of our data, we considered an interaction between TF and target only when coexpression existed between both entities, with a threshold of 0.7 for positive correlations or  $-0.7$  for negative correlations. Only interactions in which TF and target were regulated in the same cell type were considered. In addition, we only kept TF–target interactions in which the target is regulated by nitrate at the same time point or after the TF. We obtained a predicted GRN consisting of 1,630 nodes and 3,995 edges (Fig. 2A and Dataset S4). To validate the predicted network, we

used TF–target information for 33 TFs determined by the cell-based TARGET TF-perturbation system (34) in root protoplasts (9). From this information, we gathered 85,144 TF–target connections and performed a precision/recall analysis to calculate the area under the precision recall (AUPR) curve.

Our predicted network showed a significantly higher AUPR value (0.39776) than a similar network based on randomized edges (mean = 0.24486;  $P < 0.05$ , permutation test) using the TARGET data as a gold standard of validated TF–target interactions (SI Appendix, Fig. S5A). Notably, the AUPR value of our predicted network is significantly higher than a network that lacks the filters for TF–target interactions (TF and target regulated in the same cell type; TF regulated before target) (AUPR = 0.2342) and a network that lacks correlation values from our spatiotemporal data (0.14739) (SI Appendix, Fig. S5B). The differences observed in AUPR values are not due to the different number of edges of the compared networks (10,000 comparisons of the same number of edges;  $P < 0.05$ , permutation test). These analyses indicate our inferred network contains bona fide TF–target interactions and highlights the impact of using spatiotemporal transcriptomic data to determine regulatory interactions.

Our results revealed that most TF–target gene interactions were found in only one cell type (85% of the interactions), with 62% of them predicted to occur in the endodermis, highlighting this tissue as a cell type enriched in regulatory interactions ( $P$  value of  $6.2 \times 10E-445$  and 1.8-fold enrichment; number of interactions divided by the expected number of interactions, hypergeometric test) (Fig. 2A and SI Appendix, Fig. S6A). In the case of shared edges, most of them are detected among

external cell types, with 50.2% of them being shared between the epidermis, cortex, and endodermis (SI Appendix, Fig. S6B).

Accordingly, a high number of TFs were found to be nitrate regulated in the endodermis at 20 and 60 min (Fig. 2B). Importantly, the regulatory potential of endodermis-regulated TFs (expressed as the outdegree per TF) is higher in this tissue than in other tissues (Fig. 2C), suggesting a few TFs control most of the nitrate response in endodermis.

To identify important regulators of the nitrate response in the predicted network, we calculated a normalized outdegree value by dividing the TF outdegree by the number of TF–target interactions in the Plant Cistrome Database, AGRIS, and CIS-BP databases (Fig. 2D). Most of the top 10 connected TFs have a predominant role in the endodermis, except for TGA1, which has a similar number of targets across all cell types (Fig. 2D and SI Appendix, Fig. S7). This is consistent with its role as a key regulatory factor of nitrate transport and metabolic genes (8, 10–13). We found the most connected TF was *ABF3* (Fig. 2D), a member of the AREB/ABF family of TFs that participate in ABRE-dependent ABA signaling (35). Interestingly, *ABF2*, a close homolog of *ABF3*, was found third in the ranking. Although a link between ABA signaling and root responses to nitrate has been previously reported (36, 37), *ABF2* and *ABF3* have not been previously associated with the nitrate response. We found that *ABF2* and *ABF3* are rapidly induced by nitrate (at 12 or 20 min of nitrate treatment) in all cell types. *ABF2*- and *ABF3*-predicted targets are also rapidly responding to nitrate in all cell types, being either induced or repressed by nitrate. The endodermis contains most of the differentially expressed *ABF2* and *ABF3* targets, and an important number

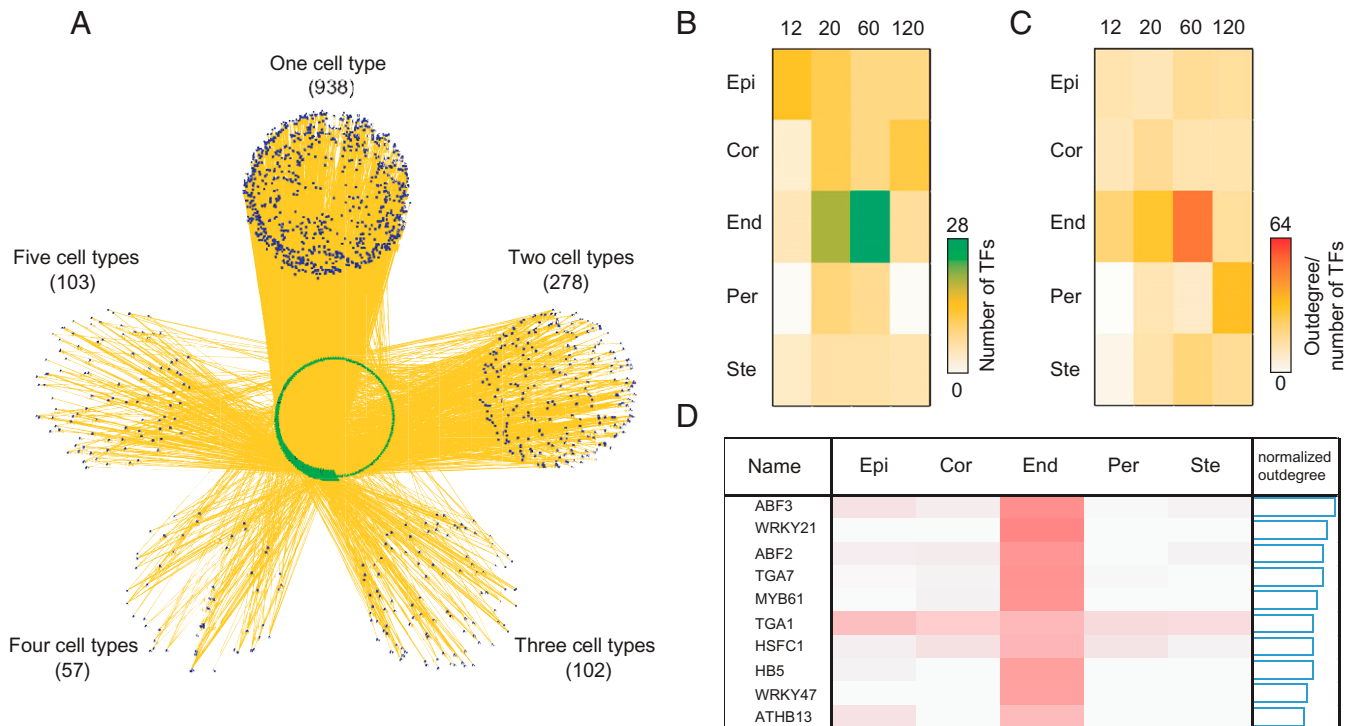


**Fig. 2.** Gene network analysis predicts the endodermis as an important site of regulatory interactions in the nitrate response. (A) Regulatory interactions between regulated TFs and targets were determined as described in the text and visualized using Cytoscape (77). Nodes in the network represent genes (green triangles: TFs; purple circles: non-TF genes) and edges represent regulatory interactions. TF targets were arranged in five groups depending on the number of cell types where a TF–target regulatory interaction is found. The number of edges show that most regulatory interactions occur in only one cell type. (B) Heatmap representation of the number of nitrate-controlled TFs from the predicted network in each cell type and time point. (C) Heatmap representation of the total outdegree of TFs divided by the total number of TFs for each cell type and time point. (D) Heatmap representation of the outdegree of the 10 most connected TFs in the network, normalized by the total interactions present in Cistrome database (31) and CIS-BP (32). The normalized outdegree bar represents the total outdegree for a given TF across all cell types normalized by the total interactions in Cistrome database and CIS-BP.

of targets are regulated only in endodermis. (Fig. 2D and *SI Appendix, Fig. S7A*).

**ABF2/ABF3 Are Important Regulators of the Endodermal Response to Nitrate.** Nine members of the AREB/ABF family have been identified in the *Arabidopsis* genome (35). However, only *ABF2* and *ABF3* are regulated by nitrate (*Dataset S2*). *ABF2* and *ABF3* respond directly to nitrate in roots since their induction is not altered in a nitrate reductase-null mutant (*SI Appendix, Fig. S8*). The nitrate regulation of these TFs depends on the NRT1.1/NPF6.3 nitrate transporter/sensor but is independent of TGA1 and TGA4, which have been previously shown to act downstream of NRT1.1/NPF6.3 to control the nitrate response (*SI Appendix, Fig. S8*) (8, 12).

Although *ABF2* and *ABF3* transcripts are expressed and regulated in the endodermis and in other cell types in response to nitrate (*Dataset S2*), we found that the ABF3 protein is expressed in the epidermis and endodermis, while ABF2 is only expressed in endodermal cells (*SI Appendix, Fig. S9*), indicating that these TFs function primarily in these cell types. These results suggest a complex posttranscriptional spatial regulation of ABF2 and ABF3 function by nitrate.

As a first step to gain insights into the regulatory function of the ABF TFs, we used the predicted GRN data to determine 11 gene targets for ABF2 and 16 genes targets for ABF3 that show regulation by nitrate on the endodermis. Using Y1H assays (38–40), we validated binding of ABF2 to the promoter of 6 of its 11 predicted targets (*Dataset S5*). Among these genes, we found *NITRITE REDUCTASE (NIR)*, which is involved in nitrite reduction, and known TFs involved in the nitrate response, including *LATERAL ORGAN BOUNDARY DOMAIN 38 (LBD38)* (41). We were not able to validate targets for ABF3 using Y1H. A possible explanation for this can be that ABF3 requires posttranslational modifications or the presence of other factors in order to bind its target genes. For example, in response to ABA, ABF factors are phosphorylated (42, 43). Nevertheless, these results support the notion that ABF2 can have a role on gene expression in response to nitrate.

In order to identify genes bound by ABF2 and ABF3 genome-wide, in an in vivo context, we performed ChIP assays using *ABF2pro::GFP:ABF2* and *ABF3pro::GFP:ABF3* lines (44) with an anti-GFP antibody in plants treated with 5 mM KCl or 5 mM  $\text{KNO}_3$  for 60 min (45). This time point was selected based on the high number of predicted ABF2/ABF3 regulatory interactions in the endodermis (Fig. 2B and C). The aggregate binding profile of target genes bound by ABF2 and ABF3 shows that TF binding occurs close to the transcription start site, as well as the transcription termination site, as previously described for other TFs (*SI Appendix, Fig. S10A*). In general, we found a good reproducibility between ChIP-seq experiments, with an intersection of 43.4 to 78.1% between biological replicates (*SI Appendix, Fig. S10B*). Importantly, the number of genes in the intersection between replicates is significant ( $P < 1\text{E-}100$ , hypergeometric test) (*SI Appendix, Fig. S10B*). A list of targets for ABF2 and ABF3 was obtained from ChIP-seq data, as described in *Methods*. We identified 1,739 and 7,696 genes bound by ABF2 and ABF3, respectively (Fig. 3A and *Dataset S6*). The sequences bound by ABF2 and ABF3 are enriched in the reported motif for these TFs obtained by DNA purification affinity sequencing (DAP-seq) (31) (1,085 of 1,732 genes with the ABF2 motif,  $P$  value of  $2.9 \times \text{E-}219$  hypergeometric test) or by protein binding microarrays (32) (954 of 1,732 genes with the ABF2 motif,  $P$  value of  $1.4 \times \text{E-}223$  and 2,123 of 7,696 genes with the ABF3 motif,  $P$  value of  $1.75 \times \text{E-}241$ , hypergeometric test).

In addition, we identified genes directly regulated by ABF2 and ABF3 on a genome-wide scale using the cell-based TARGET TF-perturbation system (45). The TARGET assay has been used previously to identify direct targets of TFs involved in the nitrate

response (6, 8, 9, 11, 14, 46). By this means, we identified 1,992 and 3,361 genes whose expression is directly regulated in root protoplasts by ABF2 and ABF3, respectively (Fig. 3A and *Dataset S6*). These ABF2- and ABF3-regulated genes captured by the TARGET assay include a significant proportion of ABF2- and ABF3-bound genes by ChIP-seq (Fig. 3A) ( $P < 2.3 \times \text{E-}67$  for ABF2 and  $P < 7.1 \times \text{E-}220$  for ABF3, hypergeometric test). By combining the lists of ABF2-regulated and ABF2-bound genes, we obtained a list of 3,332 ABF2 targets (Fig. 3A and *Dataset S6*). Similarly, we obtained a list of 9,303 ABF3 targets by combining ABF3-regulated and ABF3-bound genes (Fig. 3A and *Dataset S6*). Using ChIP or TARGET data, we can validate 22% of ABF2 and 61% of ABF3 targets predicted in the spatiotemporal network (Fig. 2A). Next, we asked whether ABF2 and ABF3 targets are enriched in genes regulated in the endodermis or any other cell type at 60 min of nitrate treatment. We found targets of ABF2 and ABF3 are highly enriched in genes regulated by nitrate in the endodermis (Fig. 3B), consistent with our network predictions (Fig. 2D). However, we also observed a significant enrichment of genes responding to nitrate in the epidermis (Fig. 3B). We found that ABF2 and ABF3 target genes are different between the epidermis and endodermis, with a higher number of target genes (*SI Appendix, Fig. S11A*), and overrepresented biological processes in the endodermis pointing at a more relevant role of ABF2 and ABF3 in this cell type (*SI Appendix, Fig. S11B*). Remarkably, ABF2 and ABF3 targets determined by either ChIP-seq or TARGET assays account for nearly 50% of the nitrate-responsive genes in the endodermis. Consistently, we found an overrepresentation of ABF2 ( $P$  value of  $3.2 \times \text{E-}8$  and 1.4-fold enrichment, hypergeometric test) and ABF3 targets ( $P$  value of  $6.7 \times \text{E-}26$  and 1.4-fold enrichment, hypergeometric test) in this cell type.

To estimate the overall contribution of ABF2 and ABF3 on nitrate-responsive genes in the endodermis, we combined the ChIP-seq and TARGET data we generated in this study and built a regulatory network in which all nodes are genes that show differential expression by nitrate treatment in the endodermis (Fig. 3C and *Dataset S7*). In this network, we were able to uncover ABF2 and ABF3 targets that were determined by both ChIP-seq and TARGET assays, constituting a high-confidence regulatory subnetwork that includes 26% of the total ABF2 and ABF3 targets of the network. In this high-confidence subnetwork, we found ABF2 target genes with known functions in the root nitrate response (metabolic gene *NADH-DEPENDENT GLUTAMATE SYNTHASE 1 [GLT1]* and TF *HRS1*) (3, 6), as well as target genes for ABF3 with roles in nitrate metabolism (*NITRATE REDUCTASE 1 [NIA1]*, *ASPARTATE AMINOTRANSFERASE 3 [ASP3]*, *GLUTAMATE DECARBOXYLASE [GAD]*), and nitrate-related TFs (*LBD38* and *TGA1*) (3, 6).

Finally, GO enrichment analysis of ABF2 and ABF3 high-confidence targets shows that these TFs regulate biological processes related to “nitrate response,” “nitrogen compound transport,” “response to abscisic acid,” and “root development,” among other processes (*SI Appendix, Fig. S12*). Altogether, these data indicate that ABF2 and ABF3 are key regulatory factors of the nitrate response in the endodermis.

**ABF2 and ABF3 Control LR Growth in Response to Changes in Nitrate Availability.** It has been reported that perturbation of TFs involved in gene-expression control in response to nitrate can alter RSA (2, 4, 5). Given the role of ABF2 and ABF3 as important regulators of the nitrate response in the endodermis, we sought to determine the possible changes in PR and LR growth elicited by nitrate in *abf2*, *abf3*, and *abf2/abf3* mutant plants. As shown in Fig. 4A, *Left*, nitrate treatment repressed PR growth in wild-type (WT) plants, as previously described (12, 30, 47). PR growth was also repressed in *abf2*, *abf3*, and *abf2/abf3* plants,

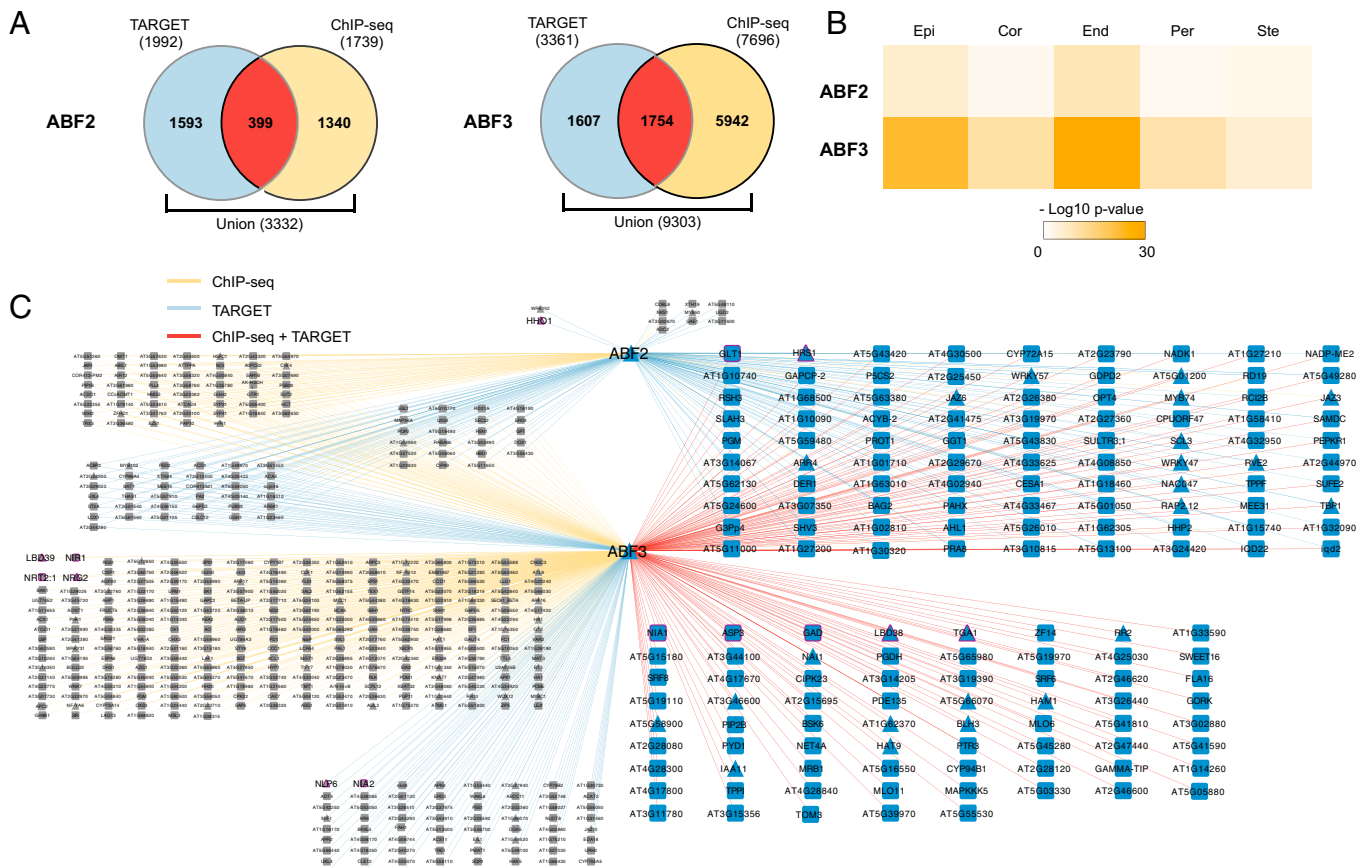


**Fig. 3.** ABF2 and ABF3 are important factors of the nitrate response in the endodermis. (A) Target genes for ABF2 and ABF3 were determined using ChIP-seq and TARGET. We show the intersection and the union between lists of targets captured for ABF2 and ABF3. (B) Heatmap showing the enrichment of ABF2 and ABF3 targets (union of the TARGET and ChIP-seq targets shown in A) in the lists of nitrate-controlled genes for each cell type, considering genes regulated after 1 h of nitrate treatment. (C) ABF2 and ABF3 regulatory network in the endodermis. Nodes represent genes with differential gene expression in response to nitrate treatment in endodermis (triangles: TFs; squares: non-TF genes). The edges represent regulatory interactions determined only by ChIP-seq (yellow edges), only by TARGET (light blue edges) or ChIP-seq and TARGET (red edges). Large blue-colored nodes represent high-confidence target genes for ABF2 and ABF3, while small gray-colored nodes represent target genes for ABF2 or ABF3 determined by ChIP or TARGET. Purple borders correspond to genes involved in nitrate signaling and metabolism according to Vidal et al. (3) and Varala et al. (6).

indicating that the ABF2/ABF3-controlled network does not have a predominant impact on nitrate-dependent PR growth. In the case of LR growth, we found that nitrate increased LR density in WT plants. However, this positive effect was absent in *abf2*, *abf3*, and *abf2/abf3* plants, and was in part due to altered nitrate-induced LR primordium development in both *abf* single-mutant plants (Fig. 4 A, Center and Right). This evidence suggests a role for ABF2/ABF3 in LR development in response to nitrate (Fig. 5). Interestingly, the altered LR response was similar in *abf* mutants and *abf2/abf3* double mutants, suggesting that ABF2 and ABF3 are not redundant factors in the control of LR development in response to nitrate.

Given that ABF2 and ABF3 are TFs that participate in the ABA signaling pathway, we next determined if altering ABA perception in the plant would have a similar impact on nitrate-dependent root growth as the *abf2/abf3* mutation. As shown in Fig. 4 B, Left, we found that the ABA receptor quintuple mutant *pyr1/pyl2/pyl4/pyl5/pyl8* (abbreviated as 12458) (48) has a similar PR response to nitrate as WT plants but exhibits an altered LR density with diminished production of LR primordia, similar to the *abf* mutants (Fig. 4 B, Center and Right). This result suggests that nitrate induces LR formation through components of the ABA pathway. Consistently, we found that CYP707A3, involved in the catabolism of ABA, and AO1 and ABA3, involved in the biosynthesis of ABA, are controlled by

the availability of nitrate in the endodermis (*SI Appendix, Fig. S13*).

In sum, our systems biology approach identified relevant TF–target gene interactions in a cell type–specific manner during the nitrate response of *Arabidopsis* roots. Our results indicate that ABF2 and ABF3 directly control a significant proportion of nitrate-responsive genes in the endodermis, and that part of these genes are involved in relevant processes that have been previously associated with root growth. Importantly, we were able to experimentally confirm ABF2 and ABF3 involvement in nitrate-controlled LR growth in *Arabidopsis*, establishing a connection between nitrate availability, the ABA signaling pathway, and root developmental processes (Fig. 5).

## Discussion

In this study, we present a high-resolution spatiotemporal transcriptional map of the nitrate response in the *Arabidopsis* root. Our results show that most nitrate-responsive genes in roots are regulated in only one cell type or time point examined, with a small proportion of the genes being broadly or persistently nitrate regulated. Similar observations have been reported in previous studies of the cell-specific response to N (19, 20), or to different stimuli, including salt stress, iron deficiency, sulfate deficiency, or low pH, where most of the genes are regulated

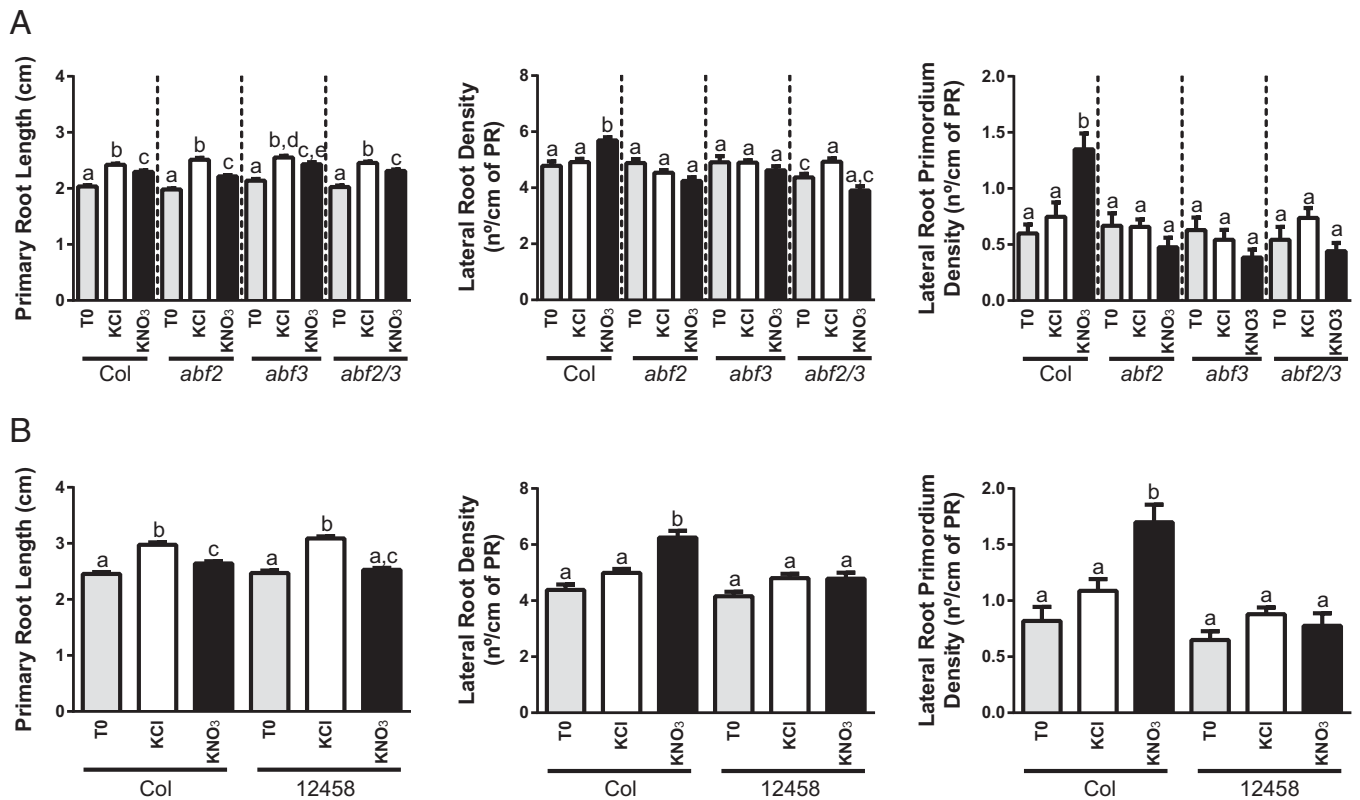


**Fig. 4.** ABF2 and ABF3 control lateral root growth in response to nitrate. *Arabidopsis* seedlings were grown for 15 d on hydroponic medium containing basal MS salts without N, supplemented with 0.5 mM ammonium succinate as sole N source and 3 mM sucrose, pH 5.7. At the onset of day 15 (T0), plants were treated with 5 mM KNO<sub>3</sub> or 5 mM KCl. After 3 d, plants were collected and root parameters were measured for KNO<sub>3</sub> or KCl treated plants. PR length was measured using the ImageJ program. Initiating (stages I to VII) and emerging LRs [stages according to Malamy and Benfey (85)], were counted using a microscope and DIC optics. LR density was then calculated dividing the total number of LRs by the PR length. For LR primordium density, only initiating LRs (stages I to VII) were considered. PR length, LR density, and LR primordium density for Col-0 WT plants, *abf2*, *abf3* and *abf2abf3* mutants (A) and for (B) Col-0 and *pyr1/pyl2/pyl4/pyl5/pyl8* quintuple mutant (abbreviated as 12458). Bars represent means with SEs. Different letters indicate statistically different means (one-way ANOVA,  $P < 0.05$ ,  $n = 30$ ).

in only one cell type (49–52). In addition, time-course transcriptome analyses of *Arabidopsis* roots in response to nitrate treatment have shown that only 33% of the nitrate-responsive genes are regulated in all time points analyzed after short times of nitrate exposure (7). Consistently, our findings indicate that gene expression in response to nitrate is highly localized and transient.

Nitrate regulation of gene expression has been described to depend mainly on the experimental context (7, 27, 53), probably due to redundancy of genes that participate in related biological processes. We found that biological processes are more consistently regulated across cell types and time points than nitrate-responsive genes. Moreover, we found that TF–target interactions are cell and time dependent, suggesting that common TFs might regulate redundant genes. This type of regulation, termed response nonredundancy, has been reported for N-responsive genes and *Sinorhizobium melliloti*–responsive genes in *Arabidopsis* roots (20). Response nonredundancy has been hypothesized to enable high temporal and spatial specificity in gene expression while maintaining a coherent control of biological processes (20).

Although changes in gene expression of a limited set of genes have been reported as early as 3 min after nitrate treatment of whole roots (7), the early response to nitrate has not been previously documented at the cell-type level. We found that all cell types analyzed show significant changes in transcript levels 12 min after the nitrate treatment, suggesting that changes in nitrate availability are sensed rapidly in all cell types.

Alternatively, a signal elicited by nitrate in a specific cell type is quickly transduced to other cell types of the root to generate a response, as previously described (19). Notwithstanding, at the earliest time point analyzed, we found enrichment of nitrate-responsive biological processes only in the epidermis. This observation suggests the outer layer of the root is the first to execute a coherent response to the nitrate signal. The putative role of the epidermis as an initial sensor of environmental cues has been reported in previous studies showing that the epidermis is the first responsive tissue to salt stress and iron deficiency (49). This is consistent with its outermost position in the root and also with the expression of nitrate transporters that can act as nitrate sensors, including NRT1.1/NPF6.3 (54) and NRT2.1 (55). Regulation of nitrate-related processes across all cell types in later time points indicates that nitrate can be imported and metabolized in each tissue. A previous example of this is the finding that the nitrate regulation of the miR167-ARF8 module in pericycle cells is mediated by glutamate, a downstream metabolite (19). Importantly, we found a coordinated temporal and spatial progression of biological processes, with hormonal and developmental processes being regulated later or in internal root layers, such as the endodermis and pericycle, root tissues that have a known function in controlling growth and development of the root system in response to stimuli (20, 47, 51, 56).

We found that the endodermis is the most nitrate-responsive tissue in terms of the number of regulated genes, indicating that transcriptomic reprogramming of this tissue is important

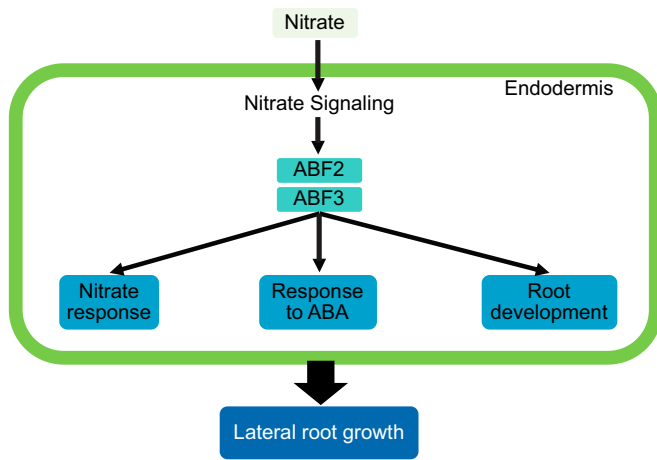


**Fig. 5.** Model for ABF2/ABF3 regulation of the nitrate response in the endodermis. Nitrate induces *ABF2* and *ABF3* transcript levels through an unknown nitrate signaling pathway in the endodermis. In turn, *ABF2* and *ABF3* directly control the expression of a relevant proportion of nitrate-responsive genes in the endodermis. Genes downstream of *ABF2* and *ABF3* in this tissue are enriched in GO terms related to nitrate response, response to ABA and root development, among other processes. Changes in gene expression mediated by the *ABF2* and *ABF3* control LR growth in response to nitrate.

for the root response to nitrate. This targeted reprogramming of specific cell transcriptomes has also been described for other stimuli; for example, the cortex is the most responsive cell type in the salt-stress response, while the stele is the most responsive cell type in the iron-starvation response (49, 51). This suggests that the organ response to a changing environment must be preceded by a fine, cell-type level adjustment of transcript levels specific to different external cues. Moreover, our GRN analysis identified the endodermis as a cellular type enriched in regulatory interactions. The most characteristic feature of the endodermis is the presence of the Casparian strip, a deposition of cell wall materials that generates selective nutrient and water loading into the vascular cylinder (57, 58). However, its functions extend to the integration of hormonal signaling, root growth, and patterning control. Interestingly the endodermis exerts its control of LR growth in a noncell-autonomous fashion by targeting adjacent tissues, such as the stele and the pericycle (59, 60). The endodermis regulates root growth by integrating different nutritional and hormonal cues into changes in developmental programs (61). For example, ABA and auxin signaling are required specifically within the endodermis for controlling LR initiation (51, 56, 59, 60). In this context, nitrate regulation of genes in the endodermis might control several aspects of root biology, such as nitrate transport to shoot tissue, as well as root architecture.

Our network analysis based on gene-expression profiles allowed us to identify candidate TFs to regulate cell-specific responses to nitrate. Importantly, the integration of space and time information positively impacted the performance of our network predictions, consistent with the highly cell- and time-specific nature of the nitrate gene-expression response. In addition, we found that TF–target interactions are highly cell specific and are mostly controlled by TFs with no previous association to the nitrate response, underscoring the importance of using spatiotemporal regulatory networks when addressing specific biological questions. Most of the hub TFs are rapidly induced or repressed by nitrate, highlighting their role in orchestrating the early nitrate response of roots, and some of them—such as *WRKY21*, *WRKY47*, *HB5*, *ATHB13*, and *MYB61*—show a specific regulation limited to one or two cell types. On the other hand, we found the *ABF2* and *ABF3* TFs that are widely nitrate-responsive but

impact transcriptional regulatory networks with a high specificity in endodermis. As described previously, commonly expressed TFs may display broad or highly cell-specific actions, and such activities may be brought to light by analyzing TFs in the context of their TF partners (62). Finally, *TGA1* and its predicted targets are broadly regulated. This shows that different regulatory mechanisms act to determine the cell specificity of the nitrate response in roots.

We determined the degree of relatedness between different cell types by analyzing specific and shared edges. We found 15% of edges are shared in at least two cell types. Most of them are common in external cell types, with more than 50% being shared between the epidermis, cortex, and endodermis. This result suggests that similar factors contribute to gene expression in response to nitrate in external cell types. However, only a fraction of all potential edges is observed in more than one cell type, and most are unique to specific cell types, with the endodermis being the most connected cell type. At least part of the high connectivity observed in this cell type might be explained by the high number of nitrate-responsive TFs and the high outdegree of these TFs.

We identified *ABF2* and *ABF3* as key regulatory factors in the root nitrate response. *ABF2* and *ABF3* are TFs that participate in ABA-mediated signal transduction pathways under stresses, such as drought and high-salinity, and during seedling growth and glucose responses (35, 44, 63). Several lines of evidence have pointed to a cross-talk between ABA and nitrate signaling in roots. For example, ABA signaling is important for LR growth and gene regulation in response to nitrate (36, 37). Nitrate can also control the ABA signaling pathway in roots by inducing the release of ABA from the endoplasmic reticulum, particularly in the endodermis (37). This increase in ABA levels is due to the induction of the  $\beta$ -*GLUCOSIDASE1* gene (*BG1*) in response to nitrate (37). Although we did not find an induction of *BG1* in any of the cell types or points analyzed, we found that *CYP707A3*, involved in the catabolism of ABA, and *AO1* and *ABA3*, involved in the biosynthesis of ABA, are controlled by the availability of nitrate in the endodermis. This finding suggests that nitrate can control ABA levels in the endodermis by different mechanisms, including its biosynthesis and catabolism, as well as its previously reported role controlling *BG1*. A meta-analysis revealed that nitrate-regulated genes are highly enriched in ABA-responsive genes (64). Consistently, there is a significant enrichment of the *cis*-regulatory elements recognized by ABA-responsive TFs in the promoter of nitrate-regulated genes (65). A connection of ABA to early nitrate-responsive genes was also previously uncovered by Krouk et al. (7) and also in genes participating in the regulatory network of N metabolism reported by Gaudinier et al. (10).

Our spatiotemporal study provides further evidence for nitrate and ABA cross-talk in roots, mediated by *ABF2* and *ABF3* in the endodermis. We found evidence that suggests that *ABF2* and *ABF3* can regulate nearly half of the nitrate-responsive genes in the endodermis, with 13% of these target genes being determined independently by ChIP-seq or TARGET analysis. Importantly, these high-confidence genes are enriched in biological processes related to root development. Among these targets, we found known genes encoding TFs controlling gene expression and RSA in response to nitrate, including *TGA1*, *LBD37*, and *HRS1* (8, 11, 12, 41, 66).

Consistent with their predicted key regulatory role in the endodermis, we found that *ABF2* and *ABF3* are important for LR development in response to nitrate. However, we did not find a role for these TFs in PR growth in response to nitrate. Similar results were obtained when studying the salt-stress response of roots. ABA signaling in the endodermis was necessary for LR growth repression but not for PR growth repression in response to NaCl treatments (51, 56), since PRs have a

higher concentration threshold for activation of ABA signaling than LR<sub>s</sub> (51).

Our analysis allowed us to determine that nitrate-responsive genes and related biological processes are coordinately regulated in space and time. Using GRN models, we found that the endodermis acts as a regulatory hub in response to nitrate. In the endodermis, ABF2 and ABF3 are TFs playing important roles in regulating the nitrate response. Additionally, our results suggest a mechanism in which nitrate might increase ABA levels within the endodermis, leading to changes in gene expression mediated by ABF2 and ABF3. These transcriptional changes ultimately lead to induction in LR initiation or emergence. These findings increase our understanding of how plants coordinate organ responses to changes in nitrate availability at the cellular level.

## Methods

**Plant Material and Growth and Treatment Conditions.** In this work, we used *Arabidopsis* lines expressing GFP in specific cells of the root, as follows: *pWEREWOLF:erGFPm* marking cells of the LR cap and epidermis, including trichoblasts and atrichoblasts in the meristematic region of the root (67); *pAt1g09750:erGFPm* (68), marking cells of the cortex except in the proximal meristematic zone; *pSCARECROW:erGFPm* marking the quiescent center and endodermis (49, 69); E3754 marking xylem-pole pericycle cells (19); and *pWOODENLEG:erGFPm* marking stele cells including pericycle and vascular cell types (70). *Arabidopsis thaliana* ecotype Col-0 was used as WT backgrounds, as indicated. Col-0 was obtained from the *Arabidopsis* Biological Resource Center mutant bank (<https://www.arabidopsis.org>). ABF2 and ABF3 simple and double mutants (*abf2/abf3*), AREB1pro:GFP-AREB1, and ABF3pro:GFP-ABF3 reporter lines were gently donated by Kazuko Yamaguchi-Shinozaki, Japan International Research Center for Agricultural Sciences, Tsukuba, Japan (44). PYR/PYL quintuple mutant *pyr1/pyl2/pyl4/pyl5/pyl8* (48) was donated by Pedro Rodriguez, Instituto de Biología Molecular y Celular de Plantas, Valencia, Spain. The nitrate transporter NRT1.1/NPF6.3 (*chl1-5*) (71), the nitrate reductase-null mutant (*nia1/Inia2*) (28), and the TGA1 and TGA4 double mutant (*tga1/4*) (72) were part of the laboratory seed stock.

*Arabidopsis* were grown hydroponically in 200 mL of medium containing 50  $\mu$ M H<sub>3</sub>BO<sub>3</sub>, 1.5 mM CaCl<sub>2</sub>, 50  $\mu$ M MnSO<sub>4</sub>, 0.08  $\mu$ M CuSO<sub>4</sub>, 0.05  $\mu$ M Na<sub>2</sub>MoO<sub>4</sub>, 0.625 mM KH<sub>2</sub>PO<sub>4</sub>, 0.75 mM MgSO<sub>4</sub>, 25  $\mu$ M ZnSO<sub>4</sub>, 5  $\mu$ M KI, 50  $\mu$ M FeSO<sub>4</sub>, 50  $\mu$ M Na<sub>2</sub>EDTA, and 0.055  $\mu$ M CoCl<sub>2</sub> supplemented with 0.5 mM ammonium succinate as N source for 2 wk. Plants were treated at the onset of day 15 with 5 mM KNO<sub>3</sub> or 5 mM KCl as control. These experimental conditions are known to elicit a robust change in gene expression and measurable changes in RSA (12, 30, 47). Root samples for KNO<sub>3</sub> and KCl treatments were collected after 12, 20, 60, and 120 min of KNO<sub>3</sub> or KCl treatment. Protoplasts were generated as previously described (19, 73, 74) and sorted with FACS using standard procedures. Total RNA was prepared using the mirVana RNA isolation kit (Ambion) from GFP<sup>+</sup> cells (~500,000 to 1,000,000 cells) and used for gene-expression analysis using the Gene 1.0 ST arrays from Affymetrix. For each cell type and treatment, we used three independent biological replicates (each replicate considering ~4,500 plants).

**Transcriptome Data Analysis.** Raw microarray data were normalized using RMA (75) on R. Gene-level expression data were analyzed using one-way ANOVA (corrected  $P \leq 0.05$ ) to determine genes differentially expressed in at least one control-treatment comparison. The expression of these genes was analyzed using a pairwise *t* test to determine in which cell or time point a significant change in gene expression was detected (corrected  $P \leq 0.05$ ).

**Network Analysis.** To generate the GRN, we gathered information of TF–target interactions from three different sources: the AGRIS database (76), Plant Cistrome Database (31), and CIS-BP (v1.02) (32). For AGRIS and the Plant Cistrome Database, interactions were directly obtained from these databases. For CIS-BP, position weight matrices associated with each TF were obtained and binding sites were predicted using meme-suite 4.1.1 with default options in promoter regions defined as 2,000 bp upstream of the transcription start site of each gene. We filtered the CIS-BP interactions intersected with AGRIS database or keeping those with a  $P \leq 1 \times 10^{-6}$ . TF–target interactions were filtered taking into consideration coexpression of TF and target in our dataset, only keeping interactions in which a correlation of  $0.7 \leq \text{cor} \leq -0.7$  and a corrected  $P \leq 0.01$  was determined. An additional filter was considered, in which an interaction between a TF and a target was kept only when the TF was

regulated at the same time point or before its target in the same cell type. The resulting network was visualized using Cytoscape (77).

**AUPR Analysis.** The AUPR analysis for validating our predicted network was performed with the TF–target pairs ordered according to the correlation data from cell type–specific data. As a gold standard, we use the TARGET assay data reported in Brooks et al. (9). We used the “evalmod” function from the “Precrec” R package (78) to calculate a receiver operating characteristic and precision-recall curves from binary values (validated or not validated) for each TF–target pair. To calculate the AUPR values for random networks, we used the “sample” function in R to create 10,000 networks that contain the same TFs and targets but with randomized edges (SI Appendix, Fig. S5). The AUPR value from our predicted network was compared to the AUPR values of 10,000 networks using the permutation test to calculate the statistical significance.

**Y1H Assay.** The Y1H assay (38, 79) was adapted from Sparks and Benfey (39). Gene promoters were cloned from Col-0 genomic DNA considering 3-kb upstream the transcription initiation site or the intergenic region, if a gene was located at a distance shorter than 3 kb. Promoters were cloned into the pMW3 and PMW2 vectors and used to transform the YM4271 yeast strain to generate the bait strain. Cloning into pMW3 generates a promoter–LacZ reporter and PMW2 generates a promoter–His growth reporter. TFs were recombined into the pDEST-AD2 $\mu$  destination vector by a gateway LR reaction. This construct was transformed directly into the bait strain and LacZ activation was determined using a colorimetric  $\beta$ -galactosidase assay. We also transformed the empty pDEST-AD-2 $\mu$  destination vector into the bait strain as a negative control. Positive interactions between TFs and promoters were determined by examining pictures from the plates. The presence of blue color, which exceeds that of autoactivation in all colonies (i.e., background levels), was used as a criteria for LacZ<sup>+</sup> interactions. His<sup>+</sup> interactions were spotted on –His–Ura–Trp plates. The colony growth was larger than that of autoactivation in all colonies. The negative control (empty pDEST-AD-2 $\mu$ ) positions did not show growth. The assays were performed in duplicate, ensuring that both clones were positive for an interaction to be determined.

**TARGET TF-Perturbation Assay in Isolated Root Cells.** The direct regulated targets of ABF2 and ABF3 were identified using the TARGET TF-perturbation assay (34), with modifications from Brooks et al. (9). The ABF2 and ABF3 TFs were cloned into pBeaconRFP\_GR plasmid (34). For protoplast generation and transfections, we used the protocols adapted from Brooks et al. (9). Briefly, *Arabidopsis* roots of 15-d-old seedlings were harvested and the cell wall was removed using cellulase and macerozyme (Yakult, Japan). For each TF construct or the empty vector control, 4 to 6 million cells were transfected and aliquoted into three replicate wells of a 24-well plate. After overnight incubation, transfected root protoplasts were treated with 5 mM KNO<sub>3</sub>. Next, to identify direct regulated targets, 35  $\mu$ M cycloheximide was added 20 min before a 10  $\mu$ M dexamethasone treatment. Transfected cells were sorted by FACS into RFP-expressing populations 3 h after dexamethasone treatment. Cells overexpressing the TF or empty vector cells were collected, RNA was extracted using the PureLink RNA Mini Kit according to the instructions of the manufacturer (Catalog #12183018A, Ambion) and RNA-sequencing (RNA-seq) libraries were prepared according to the manufacturer’s instructions using the NEBNext Ultra RNA Library Prep Kit for Illumina. Three replicates per TF were performed for the TARGET experiment. The RNA-seq libraries were multiplexed and sequenced on an Illumina NextSeq 500 platform. The RNA-seq reads were aligned to the TAIR10 genome assembly using TopHat (40) and gene expression was estimated using the GenomicFeatures/GenomicAlignments packages. The gene counts for every sample were combined in a single file, and genes differentially expressed between the TF overexpression libraries and the empty vector libraries were identified using the DESeq2 package (80) and an FDR-adjusted  $P < 0.05$ .

**ChIP Assays and Data Analysis.** ChIP assays were performed as previously described (11). Briefly, ABF2pro:GFP-ABF2 and ABF3pro:GFP-ABF3 plants were grown in the same conditions mentioned above and then were treated with 5 mM KCl or 5 mM KNO<sub>3</sub> for 1 h. Roots were collected and fixed in 1% formaldehyde for 15 min under vacuum at 25°C. Isolated chromatin was sonicated with a Bioruptor sonicator (Diagenode). A commercial antibody anti-GFP antibody (catalog #A11122, Thermo Fisher Scientific) was used for chromatin experiments. Resulting ChIP DNA for each TF and condition (KCl or KNO<sub>3</sub>) from three independent experiments was pooled and used to generate sequencing libraries using the TruSeq DNA Sample Prep Kit (Illumina). This was performed twice, to generate two biologically independent ChIP libraries per TF and condition. ChIP DNA from the input controls for each TF and condition were also used to construct libraries. Libraries were sequenced using an

Illumina NextSeq. 500 platform (Illumina). Sequencing reads obtained from ChIP DNA and Input DNA for each TF were aligned to the Arabidopsis genome using Bowtie2 and duplicated reads were removed. ChIP-seq data for each TF was compared with its partner Input DNA control and peaks were identified by MACS2 ( $q = 0.05$ ). The resulting peaks were annotated to genes using BEDtools considering 2 kb upstream of the transcription start site. To determine target genes for each TF in each condition, we considered the intersection of both biological replicates. A final list of target genes for each TF was generated by considering the union of the KCl and KNO<sub>3</sub> targets.

**RNA Isolation and qRT-PCR.** Total RNA was isolated from whole roots with PureLink RNA Mini Kit according to the manufacturer's instructions (Catalog #12183018A, Ambion). Total RNA from protoplasts was isolated using mirVana miRNA Isolation Kit, with phenol, following the manufacturer's instructions (Catalog #AM1560, Ambion). cDNA synthesis was carried out using ImProm-II Reverse Transcription System according to the instruction of the manufacturer (Catalog #A3802, Promega). qRT-PCR was carried out using the Brilliant III Ultra-Fast SYBR Green QPCR Master Mix following kit instructions (Catalog #600882, Agilent). Reactions were performed on a StepOnePlus Real-Time PCR Systems Reagents according to equipment instructions (Catalog #4376600, Applied Biosystems). Efficiencies and C<sub>q</sub> calculations were determined using LinRegPCR, a software for the analysis of qRT-PCR (v2016.1) (81). The transcript levels were normalized relative to the *ADAPTOR PROTEIN-4 MU-ADAPTIN AP4M* (At4g24550) transcript (82).

**Analysis of RSA.** *Arabidopsis* seedlings were grown in a hydroponic medium containing ammonium succinate as the sole N source as indicated in *Plant Material and Growth and Treatment Conditions*. On day 15 after sowing, plants were treated with 5 mM KNO<sub>3</sub> or 5 mM KCl for 3 d. On day 3, plants were collected and initiating and emerging LR's were counted using differential interference contrast (DIC) optics on a Nikon Eclipse 80i microscope (12, 30, 47). For PR measures, plants were scanned using an Epson Perfection V700

Photo scanner, and roots were measured using ImageJ software (83). The data were statistically analyzed in the Graph Pad Prism 5 software.

For confocal imaging, 15-d-old seedlings grown in hydroponic medium were incubated in the dark for 10 min in 10 µg/mL propidium iodide (Invitrogen) and rinsed two times in water. Seedlings were then mounted in water and imaging was performed with a FLUOVIEW FV1000 laser-scanning confocal microscope (Olympus). The tools available from the University of California, San Diego Confocal Microscopy Plugins for ImageJ software were used for image visualization.

**Data Availability.** All microarray data generated for this study were deposited in ArrayExpress (accession no. [EMTAB-9519](https://www.ebi.ac.uk/arrayexpress/experiments/EMTAB-9519)). The ChIP-seq and TARGET data generated were deposited in the Sequence Read Archive (accession no. [PRJNA750466](https://www.ncbi.nlm.nih.gov/sra/PRJNA750466)). All other study data are included in the article and/or supporting information.

**ACKNOWLEDGMENTS.** We thank Dr. Matthew D. Brooks for the helpful discussion of area under the precision recall analyses. This work is funded by Agencia Nacional de Investigación y Desarrollo (ANID) National Fund for Scientific and Technological Development Grants 1180759 (to R.A.G.), 1210389 (to J.M.A.), and 1170926 and 1211130 (to E.A.V.); ANID–Millennium Science Initiative Program, Millennium Institute for Integrative Biology Grant ICN17\_022 (to R.A.G., E.A.V., and J.M.A.); ANID PCI Redes entre Centros de Investigación Grant REDES180097 (to E.A.V.); ANID Fondo de Desarrollo de Areas Prioritarias Grant 15090007 (to R.A.G.); EvoNet Project Grant DE-SC0014377 (to R.A.G. and G.M.C.); Comisión Nacional de Investigación Científica y Tecnológica (CONICYT)-MPG 2019 Grant MPG190013 (to R.A.G.); HHMI and NIH Maximizing Investigator's Research Award 1R35GM131725 (to P.N.B.); NIH National Institute of General Medical Sciences Grant R01GM121753 (to G.M.C.); NSF Plant Genome Grant NSF-PGRP: IOS-1840761 (to G.M.C. and J.M.A.); Zegar Family Foundation Grant A16-0051 (to G.M.C.); and National Institute for Agriculture and Food Research and Technology Grant RTA2015-00014-c02-01 (to J.M.).

1. C. Masclaux-Daubresse *et al.*, Nitrogen uptake, assimilation and remobilization in plants: Challenges for sustainable and productive agriculture. *Ann. Bot.* **105**, 1141–1157 (2010).
2. C.-H. Sun, J.-Q. Yu, D.-G. Hu, Nitrate: A crucial signal during lateral roots development. *Front Plant Sci* **8**, 485 (2017).
3. E. A. Vidal *et al.*, Nitrate in 2020: Thirty years from transport to signaling networks. *Plant Cell* **32**, 2094–2119 (2020).
4. B. Liu, J. Wu, S. Yang, J. Schiefelbein, Y. Gan, Nitrate regulation of lateral root and root hair development in plants. *J. Exp. Bot.* **71**, 4405–4414 (2020).
5. M. Asim *et al.*, Nitrate signaling, functions, and regulation of root system architecture: Insights from *Arabidopsis thaliana*. *Genes (Basel)* **11**, E633 (2020).
6. K. Varala *et al.*, Temporal transcriptional logic of dynamic regulatory networks underlying nitrogen signaling and use in plants. *Proc. Natl. Acad. Sci. U.S.A.* **115**, 6494–6499 (2018).
7. G. Krouk, P. Mirowski, Y. LeCun, D. E. Shasha, G. M. Coruzzi, Predictive network modeling of the high-resolution dynamic plant transcriptome in response to nitrate. *Genome Biol.* **11**, R123 (2010).
8. J. Swift, J. M. Alvarez, V. Araus, R. A. Gutiérrez, G. M. Coruzzi, Nutrient dose-responsive transcriptome changes driven by Michaelis-Menten kinetics underlie plant growth rates. *Proc. Natl. Acad. Sci. U.S.A.* **117**, 12531–12540 (2020).
9. M. D. Brooks *et al.*, Network walking charts transcriptional dynamics of nitrogen signaling by integrating validated and predicted genome-wide interactions. *Nat. Commun.* **10**, 1569 (2019).
10. A. Gaudinier *et al.*, Transcriptional regulation of nitrogen-associated metabolism and growth. *Nature* **563**, 259–264 (2018).
11. J. M. Alvarez *et al.*, Local changes in chromatin accessibility and transcriptional networks underlying the nitrate response in *Arabidopsis* roots. *Mol. Plant* **12**, 1545–1560 (2019).
12. J. M. Alvarez *et al.*, Systems approach identifies TGA1 and TGA4 transcription factors as important regulatory components of the nitrate response of *Arabidopsis thaliana* roots. *Plant J.* **80**, 1–13 (2014).
13. J. Canales, O. Contreras-López, J. M. Álvarez, R. A. Gutiérrez, Nitrate induction of root hair density is mediated by TGA1/TGA4 and CPC transcription factors in *Arabidopsis thaliana*. *Plant J.* **92**, 305–316 (2017).
14. J. M. Alvarez *et al.*, Transient genome-wide interactions of the master transcription factor NLP7 initiate a rapid nitrogen-response cascade. *Nat. Commun.* **11**, 1157 (2020).
15. P. Guan *et al.*, Interacting TCP and NLP transcription factors control plant responses to nitrate availability. *Proc. Natl. Acad. Sci. U.S.A.* **114**, 2419–2424 (2017).
16. C. Marchive *et al.*, Nuclear retention of the transcription factor NLP7 orchestrates the early response to nitrate in plants. *Nat. Commun.* **4**, 1713 (2013).
17. A. Medici, G. Krouk, The primary nitrate response: A multifaceted signalling pathway. *J. Exp. Bot.* **65**, 5567–5576 (2014).
18. K. H. Liu *et al.*, Discovery of nitrate-CPK-NLP signalling in central nutrient-growth networks. *Nature* **545**, 311–316 (2017).
19. M. L. Gifford, A. Dean, R. A. Gutierrez, G. M. Coruzzi, K. D. Birnbaum, Cell-specific nitrogen responses mediate developmental plasticity. *Proc. Natl. Acad. Sci. U.S.A.* **105**, 803–808 (2008).
20. L. Walker *et al.*, Changes in gene expression in space and time orchestrate environmentally mediated shaping of root architecture. *Plant Cell* **29**, 2393–2412 (2017).
21. O. Contreras-López, E. A. Vidal, E. Riveras, J. M. Alvarez, T. C. Moyano, Characterization of temporal and spatial patterns of gene expression in response to nitrate in *Arabidopsis* roots. ArrayExpress. <https://www.ebi.ac.uk/arrayexpress/experiments/EMTAB-9519/>. Deposited 4 September 2020.
22. P. Pavlidis, W. S. Noble, Analysis of strain and regional variation in gene expression in mouse brain. *Genome Biol.* **2**, research0042.0041 (2001).
23. B. O. Bargmann *et al.*, A map of cell type-specific auxin responses. *Mol. Syst. Biol.* **9**, 688 (2013).
24. C. N. Shulse *et al.*, High-throughput single-cell transcriptome profiling of plant cell types. *Cell Rep.* **27**, 2241–2247 (2019).
25. K. Birnbaum *et al.*, A gene expression map of the *Arabidopsis* root. *Science* **302**, 1956–1960 (2003).
26. S. M. Brady *et al.*, A high-resolution root spatiotemporal map reveals dominant expression patterns. *Science* **318**, 801–806 (2007).
27. J. Canales, T. C. Moyano, E. Villarreal, R. A. Gutiérrez, Systems analysis of transcriptome data provides new hypotheses about *Arabidopsis* root response to nitrate treatments. *Front Plant Sci* **5**, 22 (2014).
28. R. Wang *et al.*, Genomic analysis of the nitrate response using a nitrate reductase-null mutant of *Arabidopsis*. *Plant Physiol.* **136**, 2512–2522 (2004).
29. S. Falcon, R. Gentleman, Using GOstats to test gene lists for GO term association. *Bioinformatics* **23**, 257–258 (2007).
30. E. A. Vidal *et al.*, Nitrate-responsive miR393/AFB3 regulatory module controls root system architecture in *Arabidopsis thaliana*. *Proc. Natl. Acad. Sci. U.S.A.* **107**, 4477–4482 (2010).
31. R. C. O'Malley *et al.*, Cistrome and epistrome features shape the regulatory DNA landscape. *Cell* **165**, 1280–1292 (2016).
32. M. T. Weirauch *et al.*, Determination and inference of eukaryotic transcription factor sequence specificity. *Cell* **158**, 1431–1443 (2014).
33. R. V. Davuluri *et al.*, AGRIS: *Arabidopsis* gene regulatory information server, an information resource of *Arabidopsis* cis-regulatory elements and transcription factors. *BMC Bioinformatics* **4**, 25 (2003).
34. B. O. R. Bargmann *et al.*, TARGET: A transient transformation system for genome-wide transcription factor target discovery. *Mol. Plant* **6**, 978–980 (2013).
35. Y. Fujita *et al.*, AREB1 is a transcription activator of novel ABRE-dependent ABA signaling that enhances drought stress tolerance in *Arabidopsis*. *Plant Cell* **17**, 3470–3488 (2005).
36. L. Signora, I. De Smet, C. H. Foyer, H. Zhang, ABA plays a central role in mediating the regulatory effects of nitrate on root branching in *Arabidopsis*. *Plant J.* **28**, 655–662 (2001).

37. C. A. Ondzighi-Assoume, S. Chakraborty, J. M. Harris, Environmental nitrate stimulates abscisic acid accumulation in Arabidopsis root tips by releasing it from inactive stores. *Plant Cell* **28**, 729–745 (2016).
38. A. Gaudinier *et al.*, Enhanced Y1H assays for Arabidopsis. *Nat. Methods* **8**, 1053–1055 (2011).
39. E. E. Sparks, P. N. Benfey, Identifying gene regulatory networks in Arabidopsis by in silico prediction, yeast-1-hybrid, and inducible gene profiling assays. *Methods Mol. Biol.* **1370**, 29–50 (2016).
40. C. Trapnell, L. Pachter, S. L. Salzberg, TopHat: Discovering splice junctions with RNA-Seq. *Bioinformatics* **25**, 1105–1111 (2009).
41. G. Rubin, T. Tohge, F. Matsuda, K. Saito, W. R. Scheible, Members of the LBD family of transcription factors repress anthocyanin synthesis and affect additional nitrogen responses in Arabidopsis. *Plant Cell* **21**, 3567–3584 (2009).
42. C. Sirichandra *et al.*, The Arabidopsis ABA-activated kinase OST1 phosphorylates the bZIP transcription factor ABF3 and creates a 14-3-3 binding site involved in its turnover. *PLoS One* **5**, e13935 (2010).
43. H.-C. Chang, M.-C. Tsai, S.-S. Wu, I.-F. Chang, Regulation of ABI5 expression by ABF3 during salt stress responses in Arabidopsis *thaliana*. *Bot. Stud. (Taipei, Taiwan)* **60**, 16 (2019).
44. T. Yoshida *et al.*, AREB1, AREB2, and ABF3 are master transcription factors that cooperatively regulate ABRE-dependent ABA signaling involved in drought stress tolerance and require ABA for full activation. *Plant J.* **61**, 672–685 (2010).
45. O. Contreras-López, E. A. Vidal, E. Riveras, J. M. Alvarez, T. C. Moyano, ABF2 and ABF3 as key hubs of the nitrate-regulatory network. National Center for Biotechnology Information Sequence Read Archive. <https://www.ncbi.nlm.nih.gov/Traces/study/?acc=PRJNA750466>. Deposited 28 July 2021.
46. A. Para *et al.*, Hit-and-run transcriptional control by bZIP1 mediates rapid nutrient signaling in Arabidopsis. *Proc. Natl. Acad. Sci. U.S.A.* **111**, 10371–10376 (2014).
47. E. A. Vidal, T. C. Moyano, E. Riveras, O. Contreras-López, R. A. Gutiérrez, Systems approaches map regulatory networks downstream of the auxin receptor AFB3 in the nitrate response of Arabidopsis *thaliana* roots. *Proc. Natl. Acad. Sci. U.S.A.* **110**, 12840–12845 (2013).
48. M. Gonzalez-Guzman *et al.*, Arabidopsis PYR/PYL/RCAR receptors play a major role in quantitative regulation of stomatal aperture and transcriptional response to abscisic acid. *Plant Cell* **24**, 2483–2496 (2012).
49. J. R. Dinneny *et al.*, Cell identity mediates the response of Arabidopsis roots to abiotic stress. *Science* **320**, 942–945 (2008).
50. A. S. Iyer-Pascuzzi *et al.*, Cell identity regulators link development and stress responses in the Arabidopsis root. *Dev. Cell* **21**, 770–782 (2011).
51. Y. Geng *et al.*, A spatio-temporal understanding of growth regulation during the salt stress response in Arabidopsis. *Plant Cell* **25**, 2132–2154 (2013).
52. T. L. Jackson *et al.*, Large cellular inclusions accumulate in Arabidopsis roots exposed to low-sulfur conditions. *Plant Physiol.* **168**, 1573–1589 (2015).
53. R. A. Gutiérrez *et al.*, Qualitative network models and genome-wide expression data define carbon/nitrogen-responsive molecular machines in Arabidopsis. *Genome Biol.* **8**, R7 (2007).
54. C.-H. Ho, S.-H. Lin, H.-C. Hu, Y.-F. Tsay, CHL1 functions as a nitrate sensor in plants. *Cell* **138**, 1184–1194 (2009).
55. A. Jacquot *et al.*, NRT2.1 C-terminus phosphorylation prevents root high affinity nitrate uptake activity in Arabidopsis *thaliana*. *New Phytol.* **228**, 1038–1054 (2020).
56. L. Duan *et al.*, Endodermal ABA signaling promotes lateral root quiescence during salt stress in Arabidopsis seedlings. *Plant Cell* **25**, 324–341 (2013).
57. I. Baxter *et al.*, Root suberin forms an extracellular barrier that affects water relations and mineral nutrition in Arabidopsis. *PLoS Genet.* **5**, e1000492 (2009).
58. D. E. Enstone, C. A. Peterson, F. Ma, Root endodermis and exodermis: Structure, function, and responses to the environment. *J. Plant Growth Regul.* **21**, 335–351 (2002).
59. P. Marhavý *et al.*, Targeted cell elimination reveals an auxin-guided biphasic mode of lateral root initiation. *Genes Dev.* **30**, 471–483 (2016).
60. P. Marhavý *et al.*, Auxin reflux between the endodermis and pericycle promotes lateral root initiation. *EMBO J.* **32**, 149–158 (2013).
61. J. R. Dinneny, A gateway with a guard: How the endodermis regulates growth through hormone signaling. *Plant Sci.* **214**, 14–19 (2014).
62. S. Neph *et al.*, Circuitry and dynamics of human transcription factor regulatory networks. *Cell* **150**, 1274–1286 (2012).
63. S. Kim, J. Y. Kang, D. I. Cho, J. H. Park, S. Y. Kim, ABF2, an ABRE-binding bZIP factor, is an essential component of glucose signaling and its overexpression affects multiple stress tolerance. *Plant J.* **40**, 75–87 (2004).
64. V. Araus, J. Swift, J. M. Alvarez, A. Henry, G. M. Coruzzi, A balancing act: How plants integrate nitrogen and water signals. *J. Exp. Bot.* **71**, 4442–4451 (2020).
65. D. Nero, G. Krouk, D. Tranchina, G. M. Coruzzi, A system biology approach highlights a hormonal enhancer effect on regulation of genes in a nitrate responsive “biomodule”. *BMC Syst. Biol.* **3**, 59 (2009).
66. A. Medici *et al.*, AtNIGT1/HR51 integrates nitrate and phosphate signals at the Arabidopsis root tip. *Nat. Commun.* **6**, 6274 (2015).
67. M. M. Lee, J. Schiefelbein, WEREWOLF, a MYB-related protein in Arabidopsis, is a position-dependent regulator of epidermal cell patterning. *Cell* **99**, 473–483 (1999).
68. J.-Y. Lee *et al.*, Transcriptional and posttranscriptional regulation of transcription factor expression in Arabidopsis roots. *Proc. Natl. Acad. Sci. U.S.A.* **103**, 6055–6060 (2006).
69. S. Sabatini, R. Heidstra, M. Wildwater, B. Scheres, SCARECROW is involved in positioning the stem cell niche in the Arabidopsis root meristem. *Genes Dev.* **17**, 354–358 (2003).
70. Y. Helariutta *et al.*, The SHORT-ROOT gene controls radial patterning of the Arabidopsis root through radial signaling. *Cell* **101**, 555–567 (2000).
71. Y.-F. Tsay, J. I. Schroeder, K. A. Feldmann, N. M. Crawford, The herbicide sensitivity gene CHL1 of Arabidopsis encodes a nitrate-inducible nitrate transporter. *Cell* **72**, 705–713 (1993).
72. M. Kesarwani, J. Yoo, X. Dong, Genetic interactions of TGA transcription factors in the regulation of pathogenesis-related genes and disease resistance in Arabidopsis. *Plant Physiol.* **144**, 336–346 (2007).
73. I. Antoniadis *et al.*, Cell-type-specific cytokinin distribution within the Arabidopsis primary root Apex. *Plant Cell* **27**, 1955–1967 (2015).
74. S. V. Petersson *et al.*, An auxin gradient and maximum in the Arabidopsis root apex shown by high-resolution cell-specific analysis of IAA distribution and synthesis. *Plant Cell* **21**, 1659–1668 (2009).
75. R. A. Irizarry *et al.*, Exploration, normalization, and summaries of high density oligonucleotide array probe level data. *Bioinformatics* **4**, 249–264 (2003).
76. A. Yilmaz *et al.*, AGRIS: The Arabidopsis Gene Regulatory Information Server, an update. *Nucleic Acids Res.* **39**, D1118–D1122 (2011).
77. P. Shannon *et al.*, Cytoscape: A software environment for integrated models of biomolecular interaction networks. *Genome Res.* **13**, 2498–2504 (2003).
78. T. Saito, M. Rehmsmeier, Precrec: Fast and accurate precision-recall and ROC curve calculations in R. *Bioinformatics* **33**, 145–147 (2017).
79. B. Deplancke, V. Vermeirssen, H. E. Arda, N. J. Martinez, A. J. Walhout, Gateway-compatible yeast one-hybrid screens. *CSH Protoc.* **2006**, prot0c4590 (2006).
80. M. I. Love, W. Huber, S. Anders, Moderated estimation of fold change and dispersion for RNA-seq data with DESeq2. *Genome Biol.* **15**, 550 (2014).
81. J. M. Ruijter *et al.*, Amplification efficiency: Linking baseline and bias in the analysis of quantitative PCR data. *Nucleic Acids Res.* **37**, e45 (2009).
82. T. Czechowski, M. Stitt, T. Altmann, M. K. Udvardi, W.-R. Scheible, Genome-wide identification and testing of superior reference genes for transcript normalization in Arabidopsis. *Plant Physiol.* **139**, 5–17 (2005).
83. C. A. Schneider, W. S. Rasband, K. W. Eliceiri, NIH Image to ImageJ: 25 years of image analysis. *Nat. Methods* **9**, 671–675 (2012).
84. R. A. Gutiérrez *et al.*, Insights into the genomic nitrate response using genetics and the Sungear software system. *J. Exp. Bot.* **58**, 2359–2367 (2007).
85. J. E. Malamy, P. N. Benfey, Organization and cell differentiation in lateral roots of Arabidopsis *thaliana*. *Development* **124**, 33–44 (1997).